Steepest Descent Path Study of Electron-Transfer Reactions†

Jianshu Cao‡

Department of Chemistry, Massachusetts Institute of Technology, Cambridge, Massachusetts 02139

Received: June 22, 1999; In Final Form: October 13, 1999

A nonadiabatic steepest descent path method is developed as a qualitative tool to analyze and characterize three different kinetic regimes of electron transfer. In this approach, Miller's semiclassical instanton solution and Pechukas' self-consistent treatment of nonadiabatic coupling are applied to the path integral representation of the two-state diffusion equation. The resulting steepest descent solution defines the diffusive solvent trajectory that has the highest probability to induce electron transfer. Numerical examples demonstrate curve crossing in the nonadiabatic regime, barrier crossing in the adiabatic regime, and delocalized effects in the coherent regime, thus providing a revealing picture for the crossover from the nonadiabatic to adiabatic regime and the transition from incoherent to coherent electron transfer.

I. Introduction

The steepest descent path has been widely used as a qualitative tool for interpreting the kinetics and dynamics of chemical reactions.[1−8] It is generally considered as a characteristic reaction path, which connects reactant and product through an intervening transition state with the lowest energy. For electron transfer, however, the primary concern has been the rate of change in the electronic state. While the solvent-induced polarization energy E has been considered as the collective reaction bath coordinate in the Marcus theory,[9−11] it is often treated as fluctuating white noise, which occasionally brings electronic states to degeneracy and hence induces an electronic transition. Instead of treating solvent polarization as a secondary variable, the goal of this paper is to understand various kinetic behaviors in electron transfer by identifying and characterizing the nonadiabatic steepest descent path of solvent polarization, thus providing a new perspective of electron-transfer reactions.

Though intuitively simple, the idea of steepest descent path is deeply rooted in several modern theoretical concepts. Traditionally, the steepest descent path is found by first locating a transition state, then pushing the system slightly in the forward and the backward directions of the negative normal mode, and tracing the path in the direction of the force.[7] In other words, the steepest descent path is solved from $\gamma\dot{E} = F$, subject to a pair of initial conditions: $\dot{E}_b = 0^{\pm}$, where γ is the friction coefficient and E_b is the transition state illustrated in Figure 1. Then, intuitively, this path represents the most probable pathway that the reaction can proceed. In practice, the transition state, being the saddle point on a multidimensional surface, is much more difficult to locate than the reactant or the product. Therefore, a more attractive approach is to select the steepest descent path from all of the paths connecting the reactant and product.[2,6,8] It has been suggested that the steepest descent path thus defined is the most probable Brownian trajectory with fixed-end-point boundary conditions. Indeed, by virtue of the path integral formulation of Brownian motions, the steepest descent path can be rigorously defined as the stationary path which minimizes the Onsager−Machlup action under the constraint of stationary boundary conditions at two end points.[12−14] In the context of functional analysis, the steepest descent path is simply another example of Miller's instanton concept,[15−17] and the steepest descent evaluation of the instanton rate recovers the overdamped limit of the Kramers rate.[14] This intriguing connection between the instanton solution and the steepest descent path proves to be crucial for the generalization to electron-transfer reactions in this paper.

The coupling between different electronic state surfaces drastically increases the range and complexity of the kinetic spectrum of electron transfer. Within the simple Marcus model, at least three different kinetic regimes and two crossovers between these regimes can be identified and calculated. The first important feature of electron transfer is the crossover from the nonadiabatic regime in Figure 3a ($V \ll k_BT$) to the adiabatic regime in Figure 3b ($V > k_BT$), because the increase of the electronic coupling constant V. At high temperature, the Landau−Zener expression allows us to interpolate rate constants between these two limits.[18,19] At low temperature, the rate is enhanced by quantum tunneling effects and a nonadiabatic instanton theory has been developed to account for the crossover in the quantum regime.[20] Next, when the coupling constant (V) approaches half the reorganization energy ($\lambda/2$) as in Figure 3c, there is a transition in the electronic state from the localized to the delocalized regime.[21] Similar transitions have been predicted for two-level systems coupled to low-temperature phonon modes.[22−24] It has recently been suggested that the delocalized electronic state is responsible for population oscillations observed in mixed-valence systems.[25,26] Further, a dynamic dimension can be added to the original Marcus model by treating solvent polarization as a Brownian coordinate.[27] The result is a set of two-state diffusion equations, which was first used by Zusman to treat solvent effects on electron transfer in the nonadiabatic limit and which will be used as the electron-transfer model in this paper.

Recently, we developed a general approach to describe condensed-phase dynamics: the spectral analysis method, which is based on eigenstructures of dissipative systems instead of dynamic trajectories.[28] When applied to the two-state diffusion equation, the analysis allows us to characterize multiple time scales in electron-transfer processes, including vibrational relaxation, electronic coherence, activated curve crossing, or

† This paper is dedicated to Professor Kent Wilson.

‡ E-mail: jianshu@mit.edu.

10.1021/jp992066q CCC: $18.00
Published on Web 11/05/1999

barrier crossing. Within this unified approach, observed rate behavior, biexponential and multiexponential decay, and population oscillations are different components of the same kinetic spectrum; thus, several existing theoretical models, developed for limited cases of electron transfer, can be analyzed, tested, and extended. In particular, the rate constant extracted from the analysis bridges smoothly between the adiabatic and nonadiabatic limits, and the kinetic spectrum in the large coupling regime reveals the nature of the localization−delocalization transition as the consequence of two competing mechanisms.

The nonadiabatic steepest descent path study in this paper is a complementary approach to the spectral analysis described above. The underlying theory for the new approach is based on the same principle as that in the nonadiabatic instanton solution by Cao and Voth.[20,29] Miller[16] first suggested that low-temperature quantum rate constants can be determined by the so-called bounce classical trajectory on the inverted potential energy surface, i.e., the instanton. In terms of semiclassical analysis,[15] the instanton trajectory satisfies the Euler−Lagrange equation on the periodic imaginary time axis, and the quantum fluctuations along the instanton trajectory take the form of a Gaussian functional which can be calculated through the evaluation of the Van Vleck determinant. To extend the original instanton analysis suitable for barrier tunneling to electron transfer, nonadiabatic transitions between donor and acceptor states must be incorporated into the instanton trajectory. For this purpose, the Pechukas theory of nonadiabatic collisions[30,31] provides a general prescription for treating electronic transitions and nuclear motions in a self-consistent fashion. A combination of Miller's instanton solution and Pechukas' self-consistent treatment yields the nonadiabatic instanton solution, which allows us to calculate thermal rate constants for electron transfer and to bridge smoothly between the adiabatic and nonadiabatic limits. In this paper, we again combine the two semiclassical techniques to determine the steepest descent path for electron transfer modeled as nonadiabatic diffusion processes.

The rest of the paper is organized as follows: In section II.A, we begin with a review of the Onsager−Machlup functional analysis of the steepest descent path and its analogy with the instanton solution. Next, a path integral expression of the two-state diffusion equation is derived in section II.B, followed by the formulation of the nonadiabatic steepest descent path in section II.C. Then, numerical solutions are presented in section III for a single adiabatic surface and for the three kinetic regimes of electron transfer. We conclude the paper with a summary of the findings of the paper and remarks about possible future directions.

II. Theory

A. Onsager−Machlup Action, Steepest Descent Path, and Instanton. Many physical systems can be modeled by a Brownian particle in an external potential U, described by the Smoluchowski equation, i.e., the diffusion equation,

$$\frac{\partial \rho(t)}{\partial t} = L_{\mathrm{D}}\rho(t) = D\frac{\partial}{\partial E}\left(\frac{\partial}{\partial E} + \beta\frac{\partial U}{\partial E}\right)\rho(t) \tag{1}$$

where E is the stochastic variable for the Brownian motion, $\rho(t)$ is the distribution probability, and D is the diffusion constant. The one-dimensional Fokker−Planck operator thus defined can be transformed to a Hermitian operator[32,33]

$$H_{\mathrm{s}} = -\mathrm{e}^{\beta U(E)/2} L_{\mathrm{D}} \mathrm{e}^{-\beta U(E)/2} = -D\frac{\partial^2}{\partial E^2} + U_{\mathrm{s}}(E) \tag{2}$$

which is the Shrodinger operator with an effective potential

$$U_{\mathrm{s}}(E) = \frac{D}{4}[\beta F(E)]^2 - \frac{D}{2}\beta U''(E) \tag{3}$$

where $F = -U'$ and U'' are the first- and second-order spatial derivatives of the potential, respectively. The relevant property is the probability for the particle at E at time t given the initial position at E_0, $P(t) = P(E,t;E_0,0)$, which, in the limit of infinitesimally small time interval Δ, can be explicitly evaluated as

$$\begin{aligned}\lim_{\Delta\to 0}\langle E|\mathrm{e}^{\Delta L}|E_0\rangle &= \mathrm{e}^{-\beta U(E)/2}\langle E|\mathrm{e}^{-\Delta H_{\mathrm{s}}}|E_0\rangle \mathrm{e}^{\beta U(E_0)/2} \\ &= \frac{1}{\sqrt{4\pi D\Delta}}\exp\left\{-\frac{\beta}{2}[U(E) - U(E_0)] - \frac{1}{4D\Delta}(E - E_0)^2 - \Delta U_{\mathrm{s}}\right\}\end{aligned} \tag{4}$$

Then, the probability at longer times can be constructed from the above short-time propagator, resulting in a path integral expression[34,35]

$$P(t) = \langle E|\mathrm{e}^{Lt}|E_0\rangle = \int \mathcal{D}[E(\tau)]\mathrm{e}^{-S[E(\tau)]} \tag{5}$$

where the measure is defined by

$$\int \mathcal{D}[E(\tau)] = \lim_{N\to\infty}\frac{1}{(4\pi D\Delta)^{N/2}}\prod_{i=1}^{N-1}\int \mathrm{d}E_i \tag{6}$$

with time discretization $\Delta = t/N$, and the discretized action is defined by

$$\begin{aligned}S[E_i] = \beta\frac{U(E_{\mathrm{t}}) - U(E_0)}{2} + \\ \sum_{i=1}^{N}\left\{\frac{(E_i - E_{i-1})^2}{4D\Delta} + \frac{\Delta D}{4}[\beta F(E_i)]^2 - \frac{\Delta D}{2}\beta U''(E_i)\right\}\end{aligned} \tag{7}$$

with boundary conditions at E_0 and $E_N = E$. In other words, the probability is a summation of all of the possible paths $E(\tau)$ connecting the two end points, each carrying a weight $W[E(\tau)] = \exp\{-S[E(\tau)]\}$.

Alternatively, the path integral expression in eq 5 can be derived via the Onsager−Machlup construction.[12] It is well-known that the Fokker−Planck equation in eq 1 is equivalent to the stochastic equation

$$\gamma\dot{E} = F + \gamma\xi(t) \tag{8}$$

where the friction coefficient γ is related to the diffusion constant through $\gamma D\beta = 1$, and ξ is the scaled white noise satisfying $\langle\xi(t)\rangle = 0$ and $\langle\xi(t)\ \xi(t')\rangle = 2D\delta(t-t')$. Then, the weight distribution of the noise history $\xi(\tau)$ is

$$W[\xi(\tau)] \propto \exp\left[-\frac{1}{4D}\int \mathrm{d}\tau\ \xi(\tau)^2\right] \tag{9}$$

which, when combined with eq 8, transforms into the weight for the path $E(\tau)$

$$W[E(\tau)] \propto J[E(\tau)]\mathrm{e}^{-S_{\mathrm{OM}}[E(\tau)]} \tag{10}$$

Here, the Jacobian of the transformation is $J[E(\tau)] = \exp[\int d\tau\, D\beta U''(E)/2]$, and the Onsager−Machlup functional action is

$$S_{OM}[E(\tau)] = \frac{1}{4D}\int d\tau\, [\dot{E} - \beta D F(E)]^2 \tag{11}$$

which is equivalent to eq 7 in the continuous limit.

The path integral formalism lends itself naturally to the generalization to colored noise. In particular, when the stochastic variable is Gaussian, the weight probability can be written as

$$W[E(t)] \propto \exp\left[-\frac{1}{2}\int dt_1 \int dt_2\, E(t_1)\, C^{-1}(t_1 - t_2)\, E(t_2)\right] \tag{12}$$

where $C(t-t') = \langle E(t)\, E(t')\rangle$ is the correlation function. Simpler expressions with a single time integration in the action can be obtained for exponential decay noise. Because the Fokker−Planck equation cannot be generalized to colored noise, the functional formula provides a unique framework for studying stochastic motions under correlated noise.[13,14,36,37]

An important application of the Onsager−Machlup functional is to rigorously formulate the concept of the steepest descent path, which has been understood as a characteristic reactive path connecting the reactant and product through a transition state. Following the work by Mckane and others,[14,36,37] the Euler−Lagrange equation for the Onsager−Machlup action functional, $\delta S_{OM}/\delta E(\tau) = 0$, defines the most probable path between two fixed end points, giving

$$\ddot{E} = D^2\beta^2 F(E)\, F'(E) \tag{13}$$

with $E(0) = E_0$ and $E(t) = E_t$. This equation of motion can be understood as the classical mechanics of a particle moving in an inverted effective potential $U_{eff}(E) = -\beta^2 F(E)^2/2$. For a typical double-well potential shown in Figure 1, we can identify three stationary points, corresponding to the reactant (E_a), the transition state (E_b), and the product (E_c), respectively. To proceed, we rewrite eq 13 as

$$\frac{d}{dt}(\dot{E}^2 - \beta^2 D^2 F^2) = 0 \tag{14}$$

so that the path with stationary end points $E(0) = E_a$ and $E(t) = E_c$ has zero energy and satisfies

$$\dot{E}^2 = D^2\beta^2 F^2 \tag{15}$$

This type of solution is known as the instanton, which was first discovered by Miller and has been widely used in quantum rate calculations. In Figure 1, the instanton trajectory consists of an uphill path connecting the reactant to the transition state and a downhill path connecting the transition state to the product. The uphill path is solved from the positive square root of eq 15, $\gamma\dot{E} = U'(E)$ and, on substitution into eq 11, gives

$$S_{ab} = \int_{-\infty}^{\infty} \dot{E}\beta U'(E) = \beta[U(b) - U(a)] \tag{16}$$

which recovers the Arrhenius activation formula. The downhill path is solved from the negative square root of eq 15, $\gamma\dot{E} = -U'(E)$ and, on substitution into eq 11, yields zero action. Thus, the uphill path corresponds to a thermal-activated process, whereas the downhill path corresponds to a free-descent process. The steepest descent evaluation of eq 5 requires integration over the Gaussian fluctuations around the instanton trajectory. Following general instanton analysis, we can formally write

$$P \propto \frac{t}{\sqrt{\mathrm{Det}'\, \partial^2 S}} \exp(-S_{ab}) \tag{17}$$

where the path duration t arises from the integration of the translational-invariant mode, which is a signature of the instanton solution, and the prefactor $\mathrm{Det}'\, \partial^2 S$ is a properly normalized Van Vleck determinant, excluding the zero eigenvalue.[17,20] Then, the reaction rate can be extracted from eq 17 to give

$$k \propto \frac{\exp(-S_{ab})}{\sqrt{\mathrm{Det}'\, \partial^2 S}} \tag{18}$$

which can be shown to yield the diffusion-limited rate.[14,36,37] Therefore, the steepest descent path is the instanton trajectory in the Onsager−Machlup formulation, which defines the most probable reaction path in the long-time limit and hence yields the rate constant associated with, the path. To avoid confusion, we use the term "steepest descent path" in the current context of classical Brownian trajectories and reserve the term "instanton" for quantum rate calculations, though conceptually they are the same kind of semiclassical approximation.

As a general note, the Onsager−Machlup stochastic functional formalism shares many common features with the Feynman quantum path integral formalism:

1. Because the classical trajectory is the stationary solution to quantum path integrals, the steepest descent path is the stationary solution that carries the largest weight among all of the Brownian trajectories between two fixed end points.

2. The rate calculation based on the steepest descent reaction path is the asymptotic expansion with respect to the small parameter D, whereas the instanton solution in quantum tunneling rate calculations is the asymptotic expansion with respect to the small parameter $\hbar$.

3. For white noise, the Onsager−Machlup functional is equivalent to the Fokker−Planck equation, and the Feynman path integral is equivalent to the Bloch−Redfield equation. For colored noise, there is no general way to derive differential equations; however, we can easily include multiple-time correlation within the functional formalism as in eq 12 or influence functionals.

B. Path Integral Formulation of the Two-State Diffusion Model. The solvent effect on electron transfer is often modeled as an electronic two-level system coupled to a thermal nuclear bath, with the Hamiltonian given as

$$H = H_{TLS} + H_{Bath} \tag{19}$$

Here, the two-level part of the Hamiltonian is explicitly written as

$$H_{TLS}(E) = U_1(E)|1\rangle\langle 1| + U_2(E)|2\rangle\langle 2| + V(|1\rangle\langle 2| + |2\rangle\langle 1|) \tag{20}$$

where V is the coupling constant and $U_1(E)$ and $U_2(E)$ are the two adiabatic energy surfaces. The stochastic variable E is the solvent-induced polarization energy between electronic states, which represents the collective effect of the bath−system coupling.[10] Because the electron-transfer process involves the collective motion of a large number of solvent degrees of

freedom, the functional form for the free energy surface is Gaussian, thus giving

$$U_1(E) = \frac{(E+\lambda)^2}{4\lambda} \tag{21a}$$

$$U_2(E) = \frac{(E-\lambda)^2}{4\lambda} \tag{21b}$$

where λ is the solvent reorganization energy and ϵ is the free energy bias.

Because many chemically and biologically important electron-transfer processes take place in the overdamped solvent environment, it is reasonable to treat the bath degree of freedom E as a diffusive coordinate.[27] Then, the Hamiltonian in eq 19 leads to a two-state diffusion equation

$$\frac{\partial}{\partial t}\rho(t) = \mathcal{L}\,\rho(t) = (\mathcal{L}_D + \mathcal{L}_V)\rho(t) \tag{22}$$

where $\mathcal{L}_D$ is the Fokker−Planck operator for the solvent polarization energy and $\mathcal{L}_V = [H_{TLS}]/i\hbar$ is the Liouville operator for the two-level system. Explicitly, eq 1 can be expressed in terms of the density matrix elements

$$\dot{\rho}_1 = \mathcal{L}_1\rho_1 + iV(\rho_{12} - \rho_{21}) \tag{23a}$$

$$\dot{\rho}_2 = \mathcal{L}_2\rho_2 - iV(\rho_{12} - \rho_{21}) \tag{23b}$$

$$\dot{\rho}_{12} = \mathcal{L}_{12}\rho_{12} - i\omega_{12}\rho_{12} + iV(\rho_1 - \rho_2) \tag{23c}$$

$$\dot{\rho}_{21} = \mathcal{L}_{21}\rho_{21} + i\omega_{12}\rho_{21} - iV(\rho_1 - \rho_2) \tag{23d}$$

where the Planck constant $\hbar$ is set to unity for simplicity, $\omega_{12} = U_1(E) - U_2(E) = E - \epsilon$, ρ_μ is the diagonal matrix element for electronic population, and $\rho_{\mu\nu}$, is the off-diagonal matrix element for electronic coherence. Here, $\mathcal{L}_\mu$ is defined on the free energy surface of the μth electronic state

$$\mathcal{L}_\mu = D\frac{\partial}{\partial E}\left(\frac{\partial}{\partial E} + \beta\frac{\partial U_\mu(E)}{\partial E}\right) \tag{24}$$

and $\mathcal{L}_{12}$ and $\mathcal{L}_{21}$ are defined on the averaged free energy surface

$$\mathcal{L}_{12} = \mathcal{L}_{21} = \frac{\mathcal{L}_{11} + \mathcal{L}_{22}}{2} = D\frac{\partial}{\partial E}\left(\frac{\partial}{\partial E} + \beta\frac{\partial \bar{U}(E)}{\partial E}\right) \tag{25}$$

where $\bar{U}$ is the average of the two free energy surfaces

$$\bar{U}(E) = \frac{U_1(E) + U_2(E)}{2} = \frac{E^2 + \lambda^2}{4\lambda} + \frac{\epsilon}{2} \tag{26}$$

The diffusion constant is defined as $D = \Omega\langle E^2\rangle$, where $\langle E^2\rangle = 2\lambda k_B T$ is the mean-square fluctuation of the solvent polarization energy and $\tau_D = 1/\Omega$ is the characteristic time scale of the Debye solvent. The correlation function of the solvent polarization energy is given by $\langle E(t)\,E(0)\rangle = \langle E^2\rangle \exp(-\Omega t)$. Note that because the nuclear dynamics is modeled by the Fokker−Planck operator, the possibility of vibrational coherence is excluded in the electron-transfer dynamics. This set of semiclassical two-state equations has been previously derived in different contexts by several authors.[27,38−41]

To facilitate functional analysis, we separate the real and imaginary parts of the coherent density matrix, i.e., $\mu = R\rho_{12}$ and $\nu = F\rho_{12}$, and define a vector $\boldsymbol{\rho} = [\rho_1, \rho_2, \mu, \nu]$. Then, the two-state diffusion operator can be cast into the matrix form

$$\mathcal{L} = \mathcal{L}_D + \mathcal{L}_V = \begin{pmatrix} \mathcal{L}_1 & 0 & 0 & 0 \\ 0 & \mathcal{L}_2 & 0 & 0 \\ 0 & 0 & \mathcal{L}_3 & 0 \\ 0 & 0 & 0 & \mathcal{L}_4 \end{pmatrix} + \begin{pmatrix} 0 & 0 & 0 & -2V \\ 0 & 0 & 0 & 2V \\ 0 & 0 & 0 & \omega \\ V & -V & -\omega & 0 \end{pmatrix} \tag{27}$$

where $\mathcal{L}_D$ is the diagonal diffusion matrix with $\mathcal{L}_3 = \mathcal{L}_4 = \mathcal{L}_{12}$ and $\mathcal{L}_V$ is the off-diagonal two-level electronic coupling matrix. To construct the functional expression for the two-state diffusion equation, we first write the propagator in the discretized form

$$G(t) = e^{\mathcal{L}t} = \lim_{N\to\infty}[G_V(\Delta)G_D(\Delta)]^N \tag{28}$$

with $\Delta = t/N$, $G_D(\Delta) = \exp(\mathcal{L}_D\Delta)$ and $G_V(\Delta) = \exp(\mathcal{L}_V\Delta)$. Following the derivation in the proceeding subsection, the matrix element of the diffusion propagator is given by

$$\langle E_i|G_{D,\mu}(\Delta)|E_{i-1}\rangle = \sqrt{\frac{1}{4\pi D\Delta}}\exp[-S_\mu(E_i,E_{i-1})] \tag{29}$$

with S_μ the discretized action

$$S_\mu(E_i,E_{i-1}) = \beta\frac{U_\mu(E_i) - U_\mu(E_{i-1})}{2} + \frac{(E_i - E_{i-1})^2}{4D\Delta} + \frac{\Delta D}{4}[\beta F_\mu(E_i)]^2 - \frac{\Delta\beta D}{2}U''_\mu(E_i) \tag{30}$$

The matrix of the electronic coupling propagator can also be evaluated explicitly by rewriting $\mathcal{L}_V$ as

$$\mathcal{L}_V = \begin{pmatrix} 0 & \mathbf{B} \\ \mathbf{C}^T & 0 \end{pmatrix} \tag{31}$$

with $\mathbf{B}$ and $\mathbf{C}$ denoting vectors $\mathbf{B} = [-2V, 2V, \omega]$ and $\mathbf{C} = [V, -V, -\omega]$, respectively, and T denoting the transpose of a vector. Then, the corresponding propagator is given in the closed form

$$G_V(\Delta,E) = e^{\Delta\mathcal{L}_V} = I + \frac{\sinh(g\Delta) - 1}{g}\begin{pmatrix} 0 & \mathbf{B} \\ \mathbf{C}^T & 0 \end{pmatrix} + \frac{\cosh(g\Delta) - 1}{g^2}\begin{pmatrix} \mathbf{B}\mathbf{C}^T & 0 \\ 0 & \mathbf{C}^T\mathbf{B} \end{pmatrix} \tag{32}$$

where $g^2 = \mathbf{C}^T\mathbf{B}$ and E dependence is implied through variables V and W. Putting all of the pieces together, we arrive at the path integral solution to the two-state diffusion equation

$$G(t) = \int \mathcal{D}[E(\tau)]G_V(E_N)e^{-S(E_N,E_{N-1})}\cdots G_V(E_2)e^{-S(E_2,E_1)}G_V(E_1)e^{-S(E_1,E_0)} \tag{33}$$

where $\mathcal{D}[E(t)]$ is the measure defined in eq 6. Because G_D and G_V do not commute, this path integral expression cannot be further simplified.

C. Nonadiabatic Reaction Path. As stated earlier, the steepest descent path is the most probable reactive path with the smallest Onsager−Machlup action under the stationary boundary conditions. An electron-transfer process involves both the change in electronic states and the change in nuclear coordinates. To incorporate this fact, we define the reactant state as $|a\rangle = [\delta(E+\lambda), 0, 0, 0]$ and the product state as $|c\rangle = [0,$

$\delta(E-\lambda)$, 0, 0], which are stationary on the corresponding electronic surface. Then, the electronic transition probability can be expressed as

$$P_{\mathrm{ET}} = \langle c|G(t)|a\rangle \tag{34}$$

where $G(t)$ is given in eq 33. This definition is analogous to the electronic overlap matrix introduced in the Pechukas theory for mixed classical−quantum dynamics.[31] Along the same line, we define an effective action as

$$P_{\mathrm{ET}} = \int D[E(\tau)]\mathrm{e}^{-S_{\mathrm{eff}}[E(\tau)]} \tag{35}$$

so that $\mathrm{e}^{-S_{\mathrm{eff}}}$ represents the weight associated with a nonadiabatic path. Then, following the argument in section II.A, the nonadiabatic steepest descent path can be solved from the Euler−Lagrange equation, leading to

$$\frac{\delta S_{\mathrm{eff}}}{\delta x_i} = \frac{1}{2D\Delta}(2E_i - E_{i+1} - E_{i-1}) + \frac{\Delta D\beta^2}{4}\sum_{\mu}[(\langle F_\mu F'_\mu\rangle_i + \langle F_\mu F'_\mu\rangle_{i-1}] + \frac{\beta}{2}\sum_{\mu}[\langle F_\mu\rangle_i - \langle F_\mu\rangle_{i-1}] + \Delta\omega'\langle P\rangle = 0 \tag{36}$$

where $F_\mu = F_\mu(E_i)$, $\omega' = \partial\omega(E_i)/\partial E$, and $P_{\mu\nu} = \delta_{\mu 4}\delta_{\nu 3} - \delta_{\mu 3}\delta_{\nu 4}$ is a projection operator. Here, $\langle A\rangle_i$ denotes an average over the density matrix

$$\langle A\rangle_i = \frac{\langle c|G(t,t_i)\,AG(t_i,0)|a\rangle}{\langle c|G(t,t_i)\,G(t_i,0)|a\rangle} \tag{37}$$

where the propagator G is explicitly given in eq 33 or, equivalently,

$$\langle A\rangle_i = \frac{\langle c(t_i)|A|a(t_i)\rangle}{\langle c(t_i)|a(t_i)\rangle} \tag{38}$$

where $a(t_i)$ is the forward distribution starting from the reactant, $\dot{a}(t_i) = La(t_i)$, and $c(t_i)$ is the backward distribution starting from the product, $\dot{c}(t_i) = c(t_i)\,L$. Finally, taking the limit of $\Delta \to 0$, we have the equation of motion in the continuous form

$$\ddot{E} = \beta^2 D^2\sum_{\mu}\langle F_\mu F'_\mu\rangle + D\beta\sum_{\mu}\langle[F_\mu, L_{\mathrm{V}}]\rangle + 2D\omega'\langle P\rangle \tag{39}$$

which defines the nonadiabatic steepest descent path, namely, the Brownian trajectory that is most likely to induce electron transfer. Equation 39 is the central result of the paper.

Based on the above formulation, a computational algorithm to solve the nonadiabatic steepest descent path can be designed as follows:

1. An initial guess of $E(t)$ is used as an input. The density matrices $c(t)$ and $a(t)$ are propagated according to this initial guess.

2. For the given density matrix, the Euler−Lagrange equation in eq 36 for the steepest descent path is iterated to a converged path $E(t)$.

3. The path integral expression in eq 33 is propagated forward and backward again according to the new steepest descent path to yield a new pair of $c(t)$ and $a(t)$.

4. Steps 3 and 4 are repeated until convergence is reached.

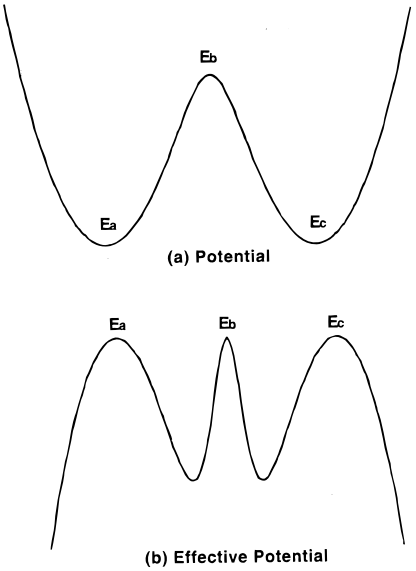

Figure 1. Typical double-well potential (a) with the corresponding effective potential (b). The potential $U_-(E)$ is the lower adiabatic potential defined in eq 40, with $\beta\lambda = 8.0$, $\beta\epsilon = 0$, and $\beta V = 1.0$, and the effective potential is defined as $U_{\mathrm{eff}} = -\beta^2F^2 = -\beta^2(U')^2$. For all of the figures in the letter, time and energy variables are scaled by the thermal energy β and $\hbar$ is taken as unity. The value of action S is calculated from eq 11.

III. Results and Discussions

A. Steepest Descent Paths on a Single Adiabatic Surface. To begin, we examine the steepest descent path on a single surface, given as

$$U_{\pm}(E) = \frac{E^2+\lambda^2}{4\lambda^4} + \frac{\epsilon}{2} \pm \sqrt{V^2 + \left(\frac{E-\epsilon}{2}\right)^2} \tag{40}$$

which is the adiabatic potential obtained by diagonalizing the two-state Hamiltonian in eq 20 with U_1 and U_2 given respectively by eqs 21a and 21b. As stated earlier, the Euler−Lagrange equation in eq 13 leads to the classical dynamics of a particle in an inverted potential $U_{\mathrm{eff}} = -\beta^2F^2(E)$. This inverted potential is plotted in Figure 1b along with the lower adiabatic potential $U_-(E)$ in Figure 1a, for $\beta V = 1$, $\beta\lambda = 8$, and $\beta\epsilon = 0$. All of the parameters and variables in this paper are scaled with β; e.g., the unit of energy or frequency is $1/\beta$ and the unit of time is β. As illustrated in Figure 1, the three stationary points are the reactant, $E_{\mathrm{a}} = -\sqrt{\lambda^2-4V^2}$; the transition state, $E_{\mathrm{b}} = 0$; and the product, $E_{\mathrm{c}} = \sqrt{\lambda^2-4V^2}$. Thus, the uphill path ($E_{\mathrm{a}} \to E_{\mathrm{b}}$) describes the activated rate process, and the downhill path ($E_{\mathrm{b}} \to E_{\mathrm{c}}$) describes the free descent path.

Ideally, by analogy with the instanton trajectory, the steepest descent path at the three stationary points has zero momentum, and hence the path duration is infinitely long. In practice, however, numerical solutions are limited by a finite path duration with a finite number of grid points. In Figure 2, the steepest descent path is plotted for the potential in Figure 1 with increasing path durations (a) $N = 100$, (b) $N = 200$, and (c) $N = 700$. The trajectories are discretized with time increment $\Delta = 0.1\beta$ and are integrated according to eq 13 with fixed boundary conditions at $E_0 = E_{\mathrm{a}}$ and $E_N = E_{\mathrm{c}}$. As the path duration increases, the momentum at the end points decreases and the trajectory converges to the steepest descent solution. The corresponding Onsager−Machlup action is evaluated according to eq 11 and is shown to converge to the exact value

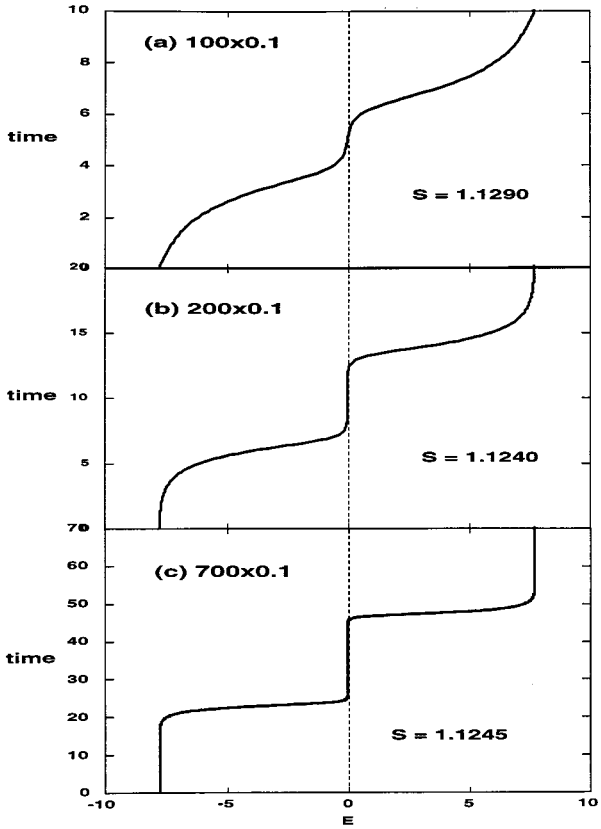

Figure 2. Plot of the steepest descent path for the potential in Figure 1 calculated with increasing path durations: (a) $N = 100$, (b) $N = 200$, and (c) $N = 700$. The trajectories are discretized with time increment $\Delta = 0.1\beta$ and are integrated according to eq 13 with fixed boundary conditions at $E_0 = E_a$ and $E_N = E_c$.

of $S_{OM} = 1.125$. At convergence, the steepest descent path consists of an uphill segment, a downhill segment, and three stationary segments. For a symmetric barrier, the steepest descent path has a reflection symmetry with respect to $E = 0$ and $t/2$. Further, the time spent on the uphill and downhill segments is almost a constant independent of the path duration. Therefore, for an ideal steepest descent path of infinite duration, the uphill and downhill segments become transient, and the stationary segments split the path with constant ratios.

B. Steepest Descent Paths for the Two-State Diffusion Equation. Because of nonadiabatic electronic coupling, the two-state diffusion equation exhibits much richer physics than the single surface diffusion equation. In Figure 3, the diabatic potential surfaces U_1 and U_2 are plotted for (a) $\beta V = 0.1$, (b) $\beta V = 1.0$, and (c) $\beta V = 4.0$, along with the upper and lower adiabatic potentials from eq 40. As discussed in the Introduction, these three sets of potential surfaces represent (a) nonadiabatic, (b) adiabatic, and (c) coherent electron transfer. Here, we present detailed numerical examples of nonadiabatic steepest descent paths for the three cases and thus illustrate the characteristic features in the three regimes.

As shown in section II.C, the nonadiabatic steepest descent path is determined from eq 36 with the initial state taken as $|a\rangle = [\delta(E+\lambda), 0, 0, 0]$ and the final state as $|c\rangle = [0, \delta(E-\lambda), 0,0]$. The path is discretized on a grid of $\Delta/\beta = 0.1$ with $N = 700$ grid points and is iterated according to the procedure described in section II.C. Except for the electronic coupling constant, the parameters used in the calculations are always taken as $\beta\lambda = 8.0$, $\beta\Omega = 1.0$, and $\beta\epsilon = 0.0$. For convenience, a straight path connecting the two end points is used as the initial guess. In the cases we studied, convergence can be achieved after 10^4-10^5 iterations.

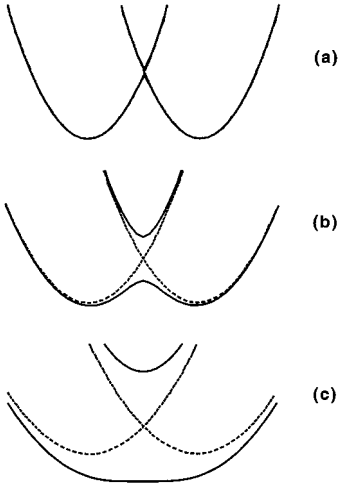

Figure 3. Adiabatic potential surfaces (solid curves) versus diabatic potential surfaces (dotted curves). The diabatic potentials are $U_1(E) = (E + \lambda)^2/(4\lambda)$ and $U_2(E) = (E - \lambda)^2/(4\lambda)$ with $\beta\lambda = 8$, and the adiabatic potentials are given by eq 40. The three diagrams represent three kinetic regimes: (a) $\beta V = 0.1$ (nonadiabatic); (b) $\beta V = 1.0$ (adiabatic); (c) $\beta V = 4.0$ (delocalized state).

1. Nonadiabatic Electron Transfer. In Figure 3a ($\beta V = 0.1$), the pair of diabatic curves are very close to the pair of adiabatic curves, except for the cusp at the curve crossing point. Thus, in the nonadiabatic limit, the electron-transfer process is confined to a small region near the curve crossing point and the resulting rate constant can be evaluated within the Marcus model and its extensions.

In Figure 4, the nonadiabatic steepest descent path is plotted for (a) $\beta V = 0.1$ and (b) $\beta V = 0.5$. Similar to Figure 3, the nonadiabatic paths consist of an uphill segment, a downhill segment, two stationary segments at the reactant and product, and a segment at the transition state. However, the segment at the transition state is not stationary but oscillatory, and the number of oscillations increases with the electronic coupling constant. This observation reflects the significant difference between barrier crossing and curve crossing. In fact, for Figure 4a, we can follow the curve crossing as first moving to the right on the diabatic surface U_1 and then crossing from U_1 to U_2 through a nonadiabatic transition. Similarly for Figure 4b, we can trace the history of curve crossing and identify multiple crossings. Therefore, electron transfer in Figure 4a is well-described by first-order perturbation theory, whereas electron transfer in Figure 4b requires higher-order corrections in terms of the electronic coupling constant. Further, the separation of activated diffusion (the uphill segment) and curve crossing (the transition state segment) confirms that the effective electron-transfer rate is a combined result of these two processes, as shown in the rate expressions derived earlier.[27,38−42]

To relate the calculated nonadiabatic steepest descent paths to the corresponding electron-transfer rate constants, we plot in Figure 5 the electronic transition probability P_{ET} in eq 34 calculated along the nonadiabatic steepest descent path as a function of the electronic coupling constant V. The Marcus rate theory predicts that the electron-transfer rate constant is proportional to the coupling constant squared, $k_{ET} \propto V^2$, in the nonadiabatic regime. This quadratic dependence is represented by the dotted curve in Figure 5, with the prefactor determined from the case of $V = 0.01$. The agreement between the two curves suggests that the steepest descent path is the dominant

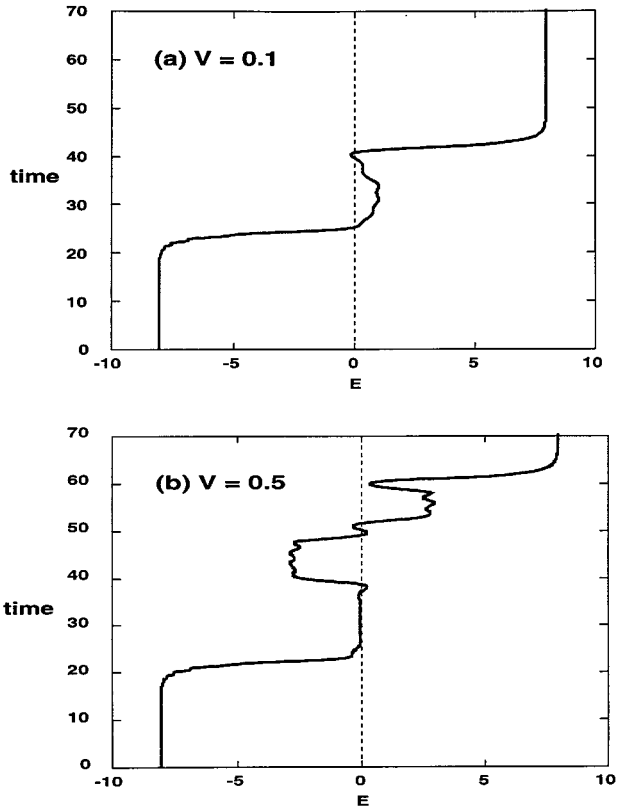

Figure 4. Plot of the nonadiabatic steepest descent path for (a) $\beta V = 0.1$ and (b) $\beta V = 0.5$. The trajectories are discretized with time increment $\Delta = 0.1\beta$ on a grid of $N = 700$ and are solved iteratively from eqs 36 and 37 with fixed boundary conditions. Except for the electronic coupling constant, the parameters used in all of the figures are taken as $\beta\lambda = 8.0$, $\beta\Omega = 1.0$, and $\beta\epsilon = 0.0$.

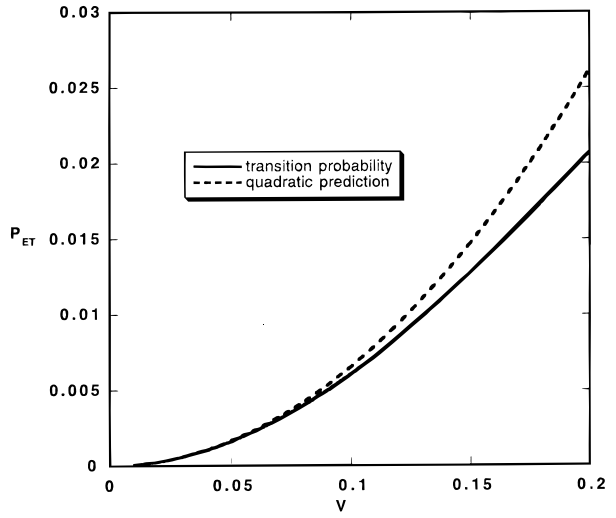

Figure 5. Plot of the electronic transition probability P_{ET} defined in eq 34 as a function of the coupling constant. The dotted curve is the quadratic golden-rule prediction (except for a constant).

path for electron transfer and provides a possible means to calculate the rate constant based on the instanton approach. As the electronic coupling constant further increases, the calculated transition probability becomes smaller than the quadratic prediction, thus supporting the possibility of the adiabatic effect and the solvent diffusion effect at a relatively large coupling constant.[28]

2. Crossover from the Nonadiabatic to the Adiabatic Regime. In Figure 3b ($\beta V = 1.0$), the two adiabatic curves are well-separated at the curve-crossing point, and the electron-transfer process becomes a thermal-activated barrier crossing on the lower adiabatic surface $U_{-}(E)$. Judging from the potential surfaces, the crossover from nonadiabatic to adiabatic electron transfer takes place at $\beta V \approx 1$. The exact nature of the crossover depends on the dynamic response time scale of the solvent.

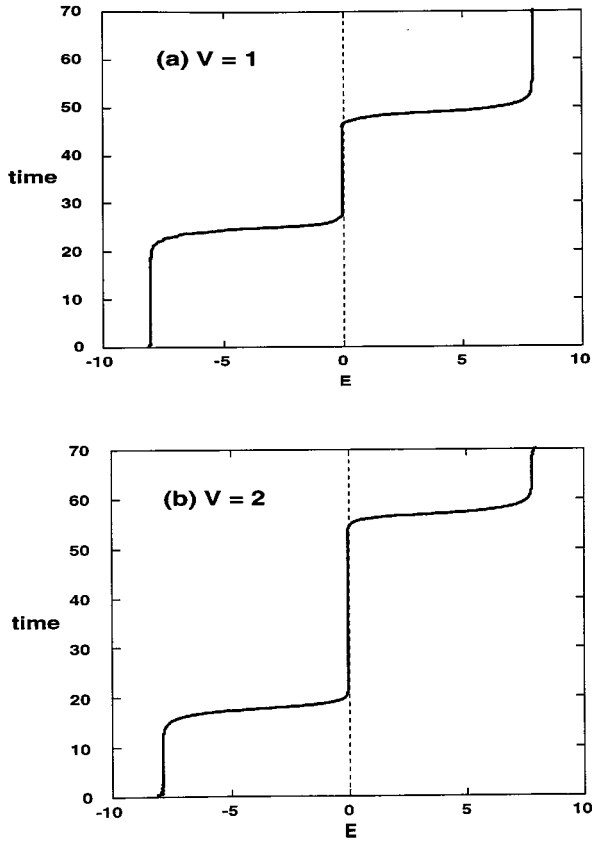

Figure 6. Plot of a nonadiabatic steepest descent path calculated with the same set of parameters as in Figure 4 except for (a) $\beta V = 1.0$ and (b) $\beta V = 2.0$.

In Figure 6, the nonadiabatic steepest descent path is plotted for (a) $\beta V = 1.0$ and (b) $\beta V = 2.0$. Not surprisingly, the resulting path in Figure 6a is nearly identical with the corresponding adiabatic path in Figure 2c, thus supporting the notion of adiabatic electron transfer at large coupling constants. As the electronic coupling constant increases to $\beta V = 2.0$ in Figure 6b, the stationary segment in the transition-state regime becomes longer because of the lowered barrier height.

These adiabatic paths in Figure 6 are significantly different from the nonadiabatic curve-crossing paths in Figure 4. However, with a different scale in Figure 7, the oscillatory behavior observed in the weak-coupling regime reappears with a much smaller amplitude. Further, the oscillation frequency is almost a constant proportional to the coupling constant V. This observation confirms the adiabatic picture proposed in an earlier paper,[25] where electronic coherence can be understood as Rabi oscillations modulated by solvent fluctuations. As seen from Figures 6 and 7, when the electronic coupling constant increases from the nonadiabatic to adiabatic regime, the frequency of nonadiabatic oscillations increases while the amplitude decreases, so that on the coarse-grained level the nonadiabatic steepest descent path appears to be the same as the corresponding adiabatic steepest descent path.

3. Transition from Incoherent to Coherent Electron Transfer. In Figure 3, as the electronic coupling constant increases from $\beta V = 1.0$ to $\beta V = 4.0$, the barrier on the lower adiabatic surface disappears; electron transfer with delocalized electronic states

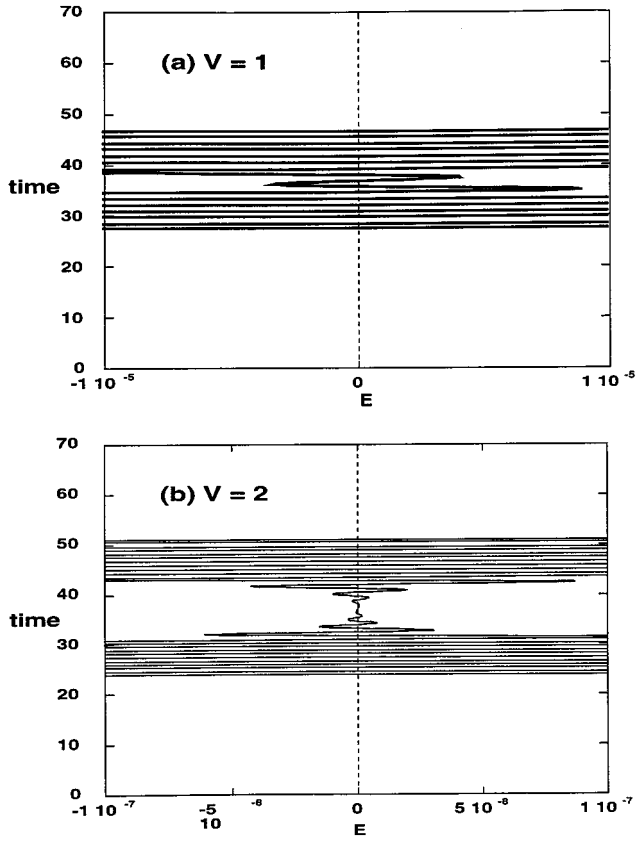

Figure 7. Magnified plot of Figure 6. The transition-state region of the steepest descent path is enlarged by a factor of 10^6 in part a and by a factor of 10^8 in part b.

becomes coherent. Though the expression in eq 40 predicts the localization−delocalization transition at half the reorganization energy, the nature of coherent electron transfer depends critically on the time scales of the system.

To understand this transition, the nonadiabatic steepest descent path is plotted in Figure 8 for (a) $\beta V = 4$ and (b) $\beta V = 6$. In comparison with the adiabatic paths in Figure 6, the stationary segment at the transition state extends over the whole time axis. Consequently, the path rises sharply to the transition state from the two end points, and the stationary segments at the reactant and the product vanish, thus indicating that the simple rate behavior no longer exists. Strictly speaking, the steepest descent path is not an instanton solution and cannot be associated with a rate process. In fact, similar to Figures 6 and 7, the extended path at the transition state is not stationary but highly oscillatory around the transition state. Next, to demonstrate the transition from localized to delocalized electron transfer, the ratio of the transition state segment to the total path duration ($t = 70\beta$) is calculated as a function of the electronic coupling constant. As shown in Figure 9, this ratio increases with the electronic coupling constant until reaching a plateau of about 80%, and the transition takes place around $V = 3.5$. Furthermore, this plateau value is also a function of the path duration. In Figure 10, steepest descent paths for $\beta V = 1.0$ are compared at several different path durations: (a) $t = 10\beta$, (b) $t = 50\beta$, and (c) $t = 500\beta$. Clearly, as the path duration increases, the ratio of the stationary segment increases until it reaches almost 99% for the case of $t = 500\beta$, indicating that for an ideal steepest descent path of infinite path duration the kinetic transition can be much sharper than that shown in Figure 9. Additionally, the effective action is almost a constant independent of N because the contribution from the extended path at the transition state sums to zero. In short, the steepest

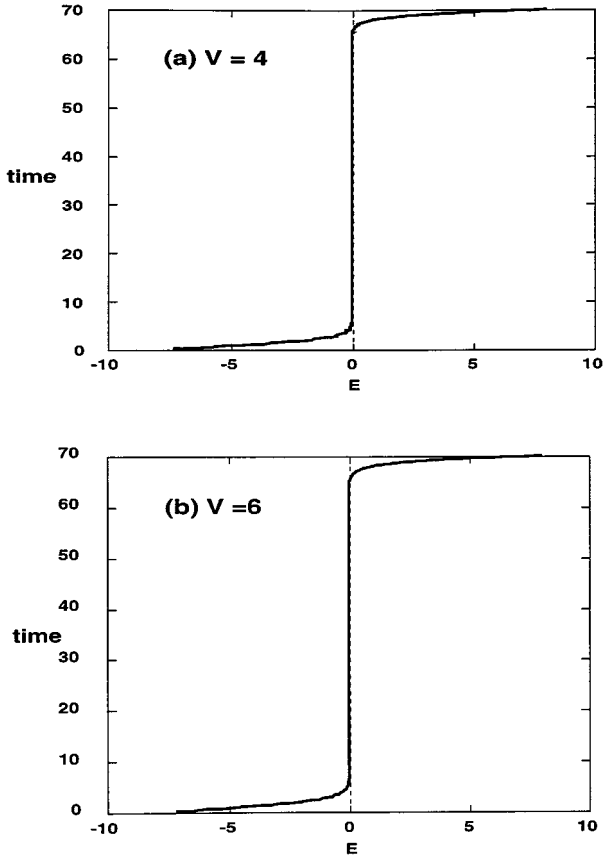

Figure 8. Plot of a nonadiabatic steepest descent path calculated with the same set of parameters as in Figure 4 except for (a) $\beta V = 4.0$ and (b) $\beta V = 6.0$.

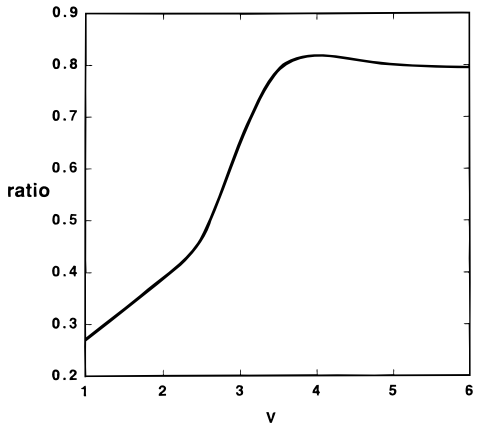

Figure 9. Plot of the ratio between the time spent at the transition state and the total path duration ($t = 70\beta$) as a function of the electronic coupling constant βV.

descent path for coherent electron transfer is a stationary coherent path which rises instantaneously from the initial and final states to the transition state.

IV. Conclusions

In summary, the nonadiabatic steepest descent path method is a useful tool to analyze and characterize electron-transfer kinetics:

1. An ideal steepest descent path on a single surface consists of three stationary segments, which are connected by two transient segments. The transient uphill segment connects the reactant to the transition state and represents the thermal-activated barrier crossing process, whereas the transient downhill

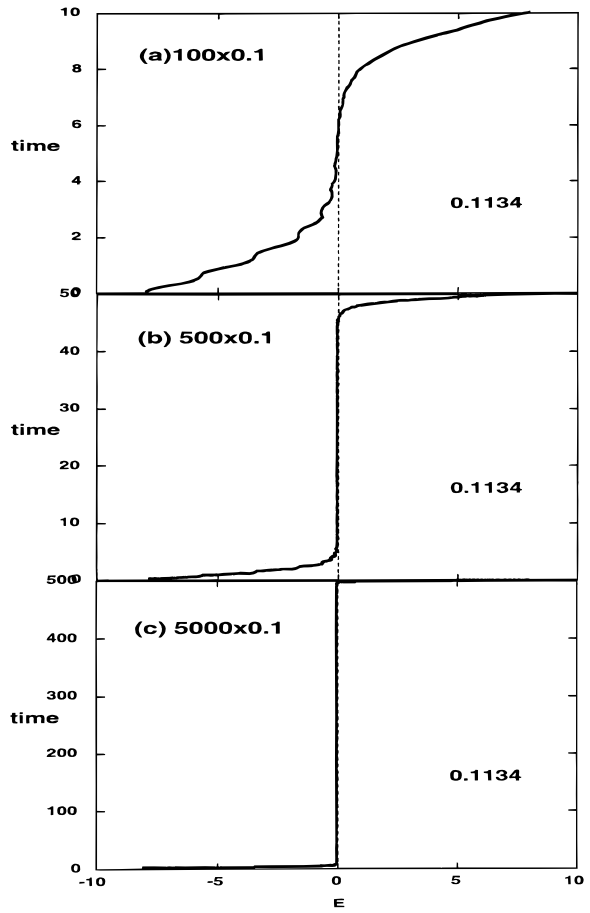

Figure 10. Plot of the nonadiabatic steepest descent path calculated for the same set of parameters as in Figure 8a but for increasing path durations: (a) $N = 100$, (b) $N = 500$, (c) $N = 5000$. The electronic transition probability P_{ET} is calculated from eq 34.

segment connects the transition state to the product and represents the free descent process.

2. In the nonadiabatic regime, the electronic transition probability P_{ET} calculated along the nonadiabatic steepest descent path depends quadratically on the electronic coupling constant, thus suggesting the possibility of calculating rate constants on the basis of the instanton approach.

3. For electron transfer with a small electronic coupling constant, the steepest descent path exhibits oscillatory crossing in the transition-state region, thus confirming that the effective electron-transfer rate is a combined result of nonadiabatic curve crossing and solvent diffusion.

4. For adiabatic electron transfer with a large electronic coupling constant, the steepest descent path is composed of Rabi oscillations with vanishing small amplitude, and the resulting envelope recovers the steepest descent path defined on the corresponding adiabatic surface.

5. For coherent electron transfer with an electronic coupling constant comparable to the reorganization energy, the transition-state segment extends over the whole path while stationary segments at the product and reactant disappear, thus indicating nonactivated behavior due to delocalized electronic states.

Though intuitive and revealing, the steepest descent path analysis at the present stage is qualitative and pictorial. Similar to the case of classical reactions, the nonadiabatic steepest descent path analysis is employed to characterize the reaction pathway and mechanism. Though this paper does not provide a detailed prescription to obtain the electron-transfer rate from the nonadiabatic steepest descent path, it is conceivable that a general frequency-dependent rate coefficient can be derived from the nonadiabatic instanton solution, as has been demonstrated by Wolynes and co-workers for reactions in slowly relaxing environments[4,5] and by McKane, Chandler, McCammon, Jonsson, and others in various contexts. Our future efforts will be directed toward developing the instanton rate solution from the nonadiabatic steepest descent path, which will allow us to calculate electron-transfer rate constants from the nonadiabatic limit to the adiabatic limit with full account of solvent relaxation effects including the possibility of nonexponential correlation.

Acknowledgment. This work is supported by the Solomon Buchsbaum AT&T Research Fund Award and by the donors of the Petroleum Research Fund, administered by the American Chemical Society.

References and Notes

(1) Ermak, D. L.; McCammon, J. A. *J. Chem. Phys.* **1978**, *69*, 1352.
(2) Edelstein, A.; Agmon, N. *J. Chem. Phys.* **1993**, *99*, 5396.
(3) Schenter, G. K.; Mills, G.; Jonsson, H. *J. Chem. Phys.* **1994**, *101*, 8964.
(4) Panchenko, A. P.; Wang, J.; Nienhaus, G. U.; Wolynes, P. G. *J. Phys. Chem.* **1995**, *99*, 9278.
(5) Wang, J.; Wolynes, P. *J. Phys. Chem.* **1996**, *100*, 1129.
(6) Dellago, C.; Bolhuis, P. G.; Csajka, F. S.; Chandler, D. *J. Chem. Phys.* **1998**, *108*, 1964.
(7) Elber, R. Reaction path studies of biological molecules. In *Recent developments in theoretical studies of proteins*; Elber, R., Ed.; World Scientific: Singapore, 1998.
(8) Elber, R.; Meller, J.; Olender, R. *J. Phys. Chem.* **1999**, *B103*, 899.
(9) Marcus, R. A. *J. Chem. Phys.* **1964**, *15*, 155.
(10) Marcus, R. A.; Sutin, N. *Biochim. Biophys. Acta* **1985**, *811*, 265.
(11) Newton, M. D.; Sutin, N. *Ann. Rev. Phys. Chem.* **1984**, *35*, 437.
(12) Onsager, L.; Machlup, S. *Phys. Rev.* **1953**, *91*, 1505.
(13) Hunt, K. L. C.; Ross, J. *J. Chem. Phys.* **1981**, *75*, 976.
(14) Bray, A. J.; McKane, A. J. *Phys. Rev. Lett.* **1989**, *62*, 493.
(15) Miller, W. H. *Adv. Chem. Phys.* **1974**, *25*, 69.
(16) Miller, W. H. *J. Chem. Phys.* **1975**, *62*, 1899.
(17) Coleman, S. The use of instantons. In *The Ways of Subnuclear Physics*; Zichichi, A., Ed.; Plenum: New York, 1979; p 805.
(18) Frauenfelder, H.; Wolynes, P. *G. Science* **1985**, *229*, 337.
(19) Straub, J. E.; Berne, B. J. *J. Chem. Phys.* **1987**, *87*, 6111.
(20) Cao, J.; Voth, G. A. *J. Chem. Phys.* **1997**, *106*, 1769.
(21) Chandler, D. In *Liquides, Cristallisation et Transition Vitreuse, Les Houches, Session LI*; Levesque, D., Hansen, J., Zinn-Justin, J., Eds.; Elsevier: New York, 1991.
(22) Harris, R. A.; Silbey, R. *J. Chem. Phys.* **1983**, *78*, 7330.
(23) Chakravarty, S.; Leggett, A. J. *Phys. Rev. Lett.* **1983**, *52*, 5.
(24) Leggett, A. J.; Chakravarty, S.; Dorsey, A. T.; Fisher, M. P. A.; Garg, A.; Zwerger, W. *Rev. Mod. Phys.* **1987**, *59*, 1.
(25) Cao, J. *Chem. Phys. Lett.* **1999**, accepted.
(26) Jung, Y.; Silbey, R. J.; Cao, J. *J. Phys. Chem.* **1999**, accepted.
(27) Zusman, L. D. *Chem. Phys.* **1980**, *49*, 295.
(28) Cao, J. *J. Chem. Phys.* **1999**, accepted.
(29) Cao, J. A unified approach for calculating quantum rate constants. In *Path Intregals from peV to TeV: 50 years after Feynman's paper*; Casalbuoni, R., Giachetti, R., Tognetti, V., Vaia, R., Verrucchi, P., Eds.; World Scientific: Singapore, 1999.
(30) Pechukas, P. *Phys. Rev. A* **1969**, *181*, 166.
(31) Pechukas, P. *Phys. Rev.* **1969**, *181*, 174.
(32) Risken, H. *The Fokker−Planck Equation*; Springer-Verlag: New York, 1984.
(33) van Kampen, N. G. *Stochastic Processes in Physics and Chemistry*; North-Holland: Amersterdam, The Netherlands, 1992.
(34) Feynman, R. P.; Hibbs, A. R. *Quantum Mechanics and Path Integrals*; McGraw-Hill Book Co.: New York, 1965.
(35) Berne, B. J.; Thirumalai, D. *Annu. Rev. Phys. Chem.* **1986**, *37*, 401.
(36) Caroli, B.; Caroli, C.; Roulet, B. *J. Stat. Phys.* **1981**, *26*, 83.
(37) Luciani, J. F.; Verga, A. D. *J. Stat. Phys.* **1988**, *50*, 567.
(38) Hynes, J. T. *J. Phys. Chem.* **1986**, *90*, 3701.
(39) Yang, D. Y.; Cukier, R. I. *J. Chem. Phys.* **1989**, *91*, 281.
(40) Sparpaglione, M.; Mukamel, S. *J. Chem. Phys.* **1988**, *88*, 3263.
(41) Garg, A.; Onuchic, J. N.; Ambegaokar, V. *J. Chem. Phys.* **1985**, *83*, 4491.
(42) Sumi, H.; Marcus, R. A. *J. Chem. Phys.* **1986**, *84*, 4894.